Supporting Information

In-situ Cross-linked 1D/3D Perovskite Heterostructure Improves Stability of Hybrid Perovskite Solar Cells for Over 3000h Operation

Ning Yang,[a] Cheng Zhu,[a] Yihua Chen,[e] Huachao Zai,[e] Chenyue Wang,[a] Xi Wang,[a] Hao Wang,[a] Sai Ma,[a] Ziyan Gao,[d] Xueyun Wang,[d] Jiawang Hong,[d] Yang Bai,[a] Huanping Zhou,[e] Bin-Bin Cui,[a, b] and Qi Chen[a, c]*

[a]Beijing Key Laboratory of Nanophotonics and Ultrafine Optoelectronic Systems, Experimental Center of Advanced Materials, School of Materials Science & Engineering, Beijing Institute of Technology (BIT), Beijing 100081, P. R. China.

[b]Advanced Research Institute of Multidisciplinary Science, Beijing Institute of Technology (BIT), Beijing 100081, P. R. China.

[c]Beijing Institute of Technology Chongqing Innovation Center, Chongqing, 401120, P. R. China

[d]School of Aerospace Engineering, BIT, Beijing 100081, P. R. China

[e]Department of Materials Science and Engineering, College of Engineering, Peking University, Beijing 100871, P. R. China

Methods

Materials.

Materials used in experiments include PbI_2 (99.999%, Sigma-Aldrich), CsI (99.9%, Sigma-Aldrich), MABr (greatcell solar), FAI (greatcell solar), MACl (greatcell solar) spiro-OMeTAD (Lumtec), SnO_2 colloid precursor (Alfa Aesar, tin(iv) oxide, 15%in H_2O colloidal dispersion), N, N-dimethylformamide (DMF; 99.99%, Sigma-Aldrich), dimethylsulfoxide (DMSO; 99.5%, Sigma-Aldrich), isopropanol (99.99%, Sigma-Aldrich), chlorobenzene (99.9%, Sigma-Aldrich), acetone (AR Beijing Chemical Works), ethanol (AR Beijing Chemical Works), aminomethane (CP Beijing Chemical Works), hydrogen iodide (57%, Aladdin Industrial Corporation) and ITO substrate (Shanghai B-Tree Tech. Consult.).

The details for synthesizing PAI.

A typical reaction entailed mixing 7.5 mL of propargylamine into 20.0 ml of isopropanol (IPA) cooled in an ice bath. A cold (~4 ^{o}C, stored in a fridge prior) solution of 12.3 ml of 57% HI (0.9 mol of HI) is added dropwise to the cooled propargylamine/PAI mixture. This mixture is left to react for 2 h, slowly warming up to room temperature. The solvent is then evaporated under reduced pressure, and the remaining white solid is left to dry for an additional 30 min under mild heating and vacuum (the temperature was maintained at 70 ^{o}C max to evaporate any water from the HI solution). The solid is then stirred in diethyl ether for 10-15 min before being filtered and wash five times with more diethyl ether. This washed solid white powder is then recrystallized by dissolving it in boiling IPA and subsequently reprecipitating with the diethyl ether. The recrystallized solid is isolated via vacuum filtration, washed an additional three times with diethyl ether, and then held under a vacuum for 16 h before being brought into a nitrogen glovebox for storage and use.

Synthesis of 1D perovskitoid single crystals.

PbI_2 (1.0 mmol, 461.0 mg) powder was dissolved in a mixture of 4.0 mL 48 wt.% aqueous HI solution by heating 60 °C under constant magnetic stirring for about 5 min, forming a clear yellow solution. Subsequent addition of (2.0 mmol, 365.9 mg) solid $C_3H_5N{\cdot}HI$ to the hot solution. The stirring stopped, and the solution was left to cool to R. T. and set up in vapor diffusion chambers with diethyl ether. Colorless and flake-shaped crystals of 1D perovskitoid were obtained through diffusion of diethyl ether into this solution over 24 h in a moderate yield (about 55%).

CCDC 1899064 contains the supplementary crystallographic data for this paper. These data can be obtained free of charge from The Cambridge Crystallographic Data Centre via www.ccdc.cam.ac.uk/ data_request/cif .

Device fabrication.

1. Solar cell device fabrication.

The ITO substrate was cleaned with ultrapure water, acetone, ethanol and isopropanol successively. The tin (IV) oxide colloidal dispersion (SnO_2, 15% in H_2O colloidal dispersion) was purchased from Alfa Aesar. The precursor solution was diluted by H_2O to 2.67%. After 45 min of ultraviolet–O_3 treatments, a SnO_2 nanocrystal solution was spin-coated on the substrate at 4,000 rpm for 30 s to form a 50-nm-thick film, which was then annealed at 150 °C for 30 min in ambient air.

To prepare the PbI_2 and organic cation precursors, 691.5 mg of PbI_2 and 15 mg of CsI were dissolved in 1.0 mL of mixture solvent of DMF: DMSO (9.5:0.5 V:V) and then annealed on a hot plate at 70 °C for 2 h with vigorous stirring. In all, 90 mg of FAI, 9mg of MABr, and 9mg of MACl were dissolved in 1 mL of isopropanol and then continuously stirred for 2 h at room temperature. To prepare the PAI solution, the PAI solution was dissolved in IPA with different concentrations ranging from 0 mg/mL to 6 mg/mL and then continuously stirred for 2 h at room temperature.

The typical sequent-step method[12] was employed to fabricate the perovskite film. First, the PbI_2 precursor was spin coated on the SnO_2 substrate in an N_2 glove box at 2500 rpm for 30 s (accelerated speed 6000 rpm·s^{-1}) and then annealed at 70 °C for 1 min in an N_2 glove box. Then, the organic cation precursor was spin-coated on the PbI_2 film at 2900 rpm for 30 s (accelerated speed 6000 rpm·s^{-1}) in an N_2 glove box. Finally, the film was kept under vacuum for 5 min and annealed at 150 °C for 30 min in ambient air to form the perovskite film. For 1D/3D perovskite film, the PAI solution was spin-coated on ITO/SnO_2/3D at 3000 rpm for 30 s in a nitrogen glovebox. For cross-linked 1D/3D, the 1D/3D perovskite film is further transfer to a pre-heated hot-plate and annealed at 150 °C 5 min to promote the cross-linking of PA.

The Spiro-OMeTAD solution was first prepared by dissolving 75 mg of Spiro-OMeTAD, 17.5 μL of a stock solution of 520 mg·mL^{-1} LiTFSI/acetonitrile, and 30 μL of tBP in 1mL of chlorobenzene. Then the Spiro-OMeTAD precursor was spin-coated at 3000 rpm for 30 s

(accelerated speed 6000 rpm·s^{-1}) in an N_2 glove box. Finally, 100 nm thick gold was thermally evaporated as a counter electrode under a pressure of 1×10^{-4} Pa on top of the Spiro-OMeTAD films to form the back contact by using a shadow mask to pattern the electrode.

2. Devices fabrication for EIS, IMPS and IMVS measurements

The device structure of EIS, IMPS and IMVS is the same as that of solar cells

3. Devices fabrication for SCLCmeasurement

The structure of the device was ITO/perovskite or perovskite heterostructure/Au. The ITO substrate was treated by UV-O_3 for 30 min, FAMACs mixed perovskite film was deposited on the ITO substrate by spin-coating. After the perovskite annealing, 150 nm Au was thermally evaporated as counter electrode.

4. Samples of c-AFM preparation

The structure of the sample was ITO/perovskite. The ITO glass substrate was treated by UV-O_3 for 30 min, FAMACs mixed perovskite film was deposited on the ITO substrate by spin-coating. Then perovskite annealing treatment is carried out.

Characterization.

Scanning electron microscope (SEM) images were obtained by Hitachi S4800 field-emission scanning electron microscopy. Depth resolved GIXRD were characterized using a Rigaku Smart Lab five-axis X-ray diffractometer at 45 kV and 200 mA, equipped with Cu Kα radiation (λ = 1.54050 Å), parallel beam optics and a secondary graphite monochromator. Before the test, the X-ray diffraction on well recrystallized LaB6 powders was used for subtle alignment of instrument, the acceptable LaB6 peak shift is less than 0.01° in 2θ comparing to its JCPDF file. For the residual stress tests, a slow scan rate of 0.12° min^{-1} was carried out to ensure fine structural information. Single crystal powder XRD and perovskite film XRD were measured using a Bruker D8 Advanced, equipped with Cu Kα radiation (λ = 1.54060 Å). The UV-visible absorption spectra were recorded with a UV-visible spectrophotometer

(Agilent 8453). Steady-state photoluminescence (PL) spectra were characterized by FLS980 (Edinburgh Instruments Ltd.), equipped with a Xe lamp, a liquid nitrogen cryostat (Oxford Instruments, OptistatDN-V), and a photomultiplier tube (PMT) detector. The excitation wavelength was 470 nm. The picosecond pulsed diode laser (EPL-470, Edinburgh Instruments Ltd.) was used to measure PL lifetime with a repetition rate of 0.2 MHz, a pulse width of 91.5 ps, a excitation fluence of ~30 $nJ \cdot cm^{-2}$, and maximum average power of 5 mW. The electrochemical impedance spectroscopy (EIS) was determined by the electrochemical workstation (Germany, Zahner Company) in dark without applied bias, according to frequency parameter from 1MHz to 100 Hz. IMPS and IMVS was determined by the electrochemical workstation (Germany, Zahner Company), employing light emitting diodes driven by Export (Germany, Zahner Company). c-AFM was measured with a bias voltage of 2 V under illumination using a MFP-3D bio (Oxford Instruments Asylum Research Inc.) with a NSG01/Pt probe. ^{1}H NMR spectra were measured using a Bruker AVANCE III 300 MHz NMR Spectrometer in designated deuterated solvent. The current density-voltage characteristics of photovoltaic devices were obtained using a Keithley 2400 source-measure unit. The photocurrent was measured under AM1.5G illumination at 100 $mW \cdot cm^{-2}$ under a Newport Thermal Oriel 91192 1000 W solar simulator. The J-V measurements were carried out in ambient air. The sweep speed was fixed at 40 $mV \cdot s^{-1}$ (step 0.02 V, delay time 500 ms). The shading mask and one of our best device were sent to an accredited PV calibration laboratory (Newport, USA) for certification. The active area was defined as 0.09408 cm^2. All The J-V measurements were conducted under Xeon lamps, and only MPP tracking experiment and the photo-stability experiment used LED white light lamps for aging. External quantum efficiencies (EQE) were obtained by an Enli Technology (Taiwan) EQE measurement system.

The cross-linking process

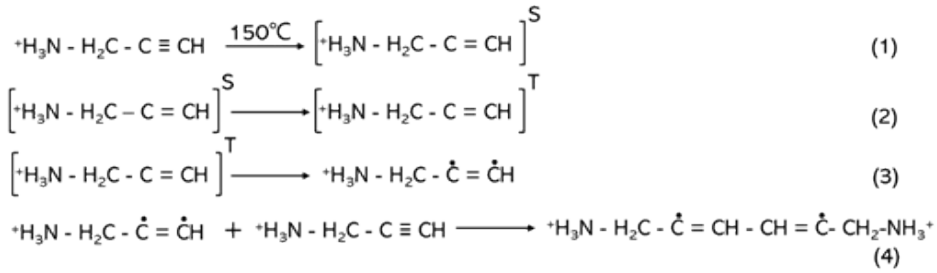

The terminal alkynyls are promoted to an excited singlet state by heating for 5 min at 150 °C (1), which is followed by intersystem crossing into the triplet state (2) and subsequent formation of radicals on the alkynyl carbons (3). The radicals can then form new covalent bonds with other nearby alkynyl groups on adjacent or opposite ligands (depending on the geometry at the interface), and the reaction propagates.

SCLC calculation

SCLC measurements of the prepared capacitor-like devices were made by sandwiching the perovskite films between ITO and Au electrodes. The J-V characteristics were recorded under dark condition, which was well fitted by the Mott-Gurney Law: $J = (9/8)\varepsilon\varepsilon^0\mu(V_2/L_3)$[13]. where L is the thickness of the perovskite, V is applied voltage, ε^0 is the vacuum permittivity, and ε (=32 measured in single crystal samples) is the relative dielectric constant of perovskite. The dielectric constant is average in the frequency range from 100 kHz to 1 MHz (plateau region), and V is the voltage drop across the device.

EIS measurement discussion

EIS examined the carrier transport dynamics at the perovskite/HTL and perovskite heterostructure /HTL interfaces. We obtained corresponding Nyquist plots of reference, 1D/3D perovskite heterostructure and in-situ cross-linked 1D/3D perovskite heterostructure solar cells in dark without applied bias along with the equivalent circuit (Fig. S9). The Nyquist plots show two arcs of high and low frequencies. The high frequency arc is generally related to charge transfer retention (R_{ct}) and the corresponding capacitance, while charge transfer is related to the interface behavior between perovskite and carrier transport layer. The arc in the low-frequency

region is designated as the combination of Recombination Resistance (R_{rec}). That is, the first ring and the solid axis typically represent the series resistance Rs of the device, which is influenced by the ITO substrate in contact with the external wire.

IMPS and IMVS test analysis

The charge transfer time (τ_T) can be calculated by IMPS results. As shown in Figure S10, with the increase of potential-modulating light intensity, compared with 1D/3D and reference, the τ_T of cross-linked 1D/3D is always the smallest, indicating that charge transmission is the fastest in cross-linked 1D/3D devices. The IMVS experiment was performed under open circuit conditions to assess charge recombination rate or charge lifetime. Fig. S11 shows the change of the recombination time constant (τ_R) of the three devices with the increase of potential-modulating light intensity. The τ_R of the device containing Cross-linked 1D/3D stacking is larger than that of the pristine device and 1D/3D device, indicating that the lower recombination rate. These two time constants can be used to further estimate the charge collection efficiency (ηcc) according to the following equation:

$$\eta cc = 1 - \tau_T / \tau_R$$

It is a decisive factor in evaluating the performance of PSCs. The higher the charge collection efficiency, the higher the cell efficiency. The parameters obtained from the IMPS and IMVS experiments are shown in Fig. S12. Clearly, the PSC with Cross-linked 1D/3D stacking shows higher ηcc values at all potential-modulating light intensities. The higher the ηcc, the more efficient is a cell, in accordance with the device performance.

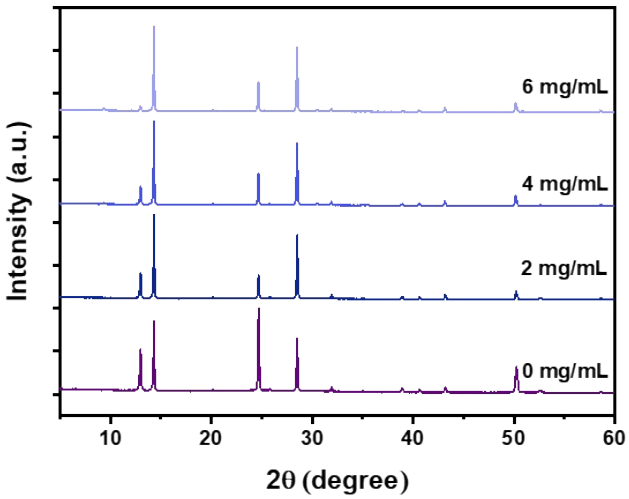

Fig. S1. XRD spectras for 1D/3D perovskite films with different PAI concentrations, concentration of 0, 2, 4 and 6 mg/mL.

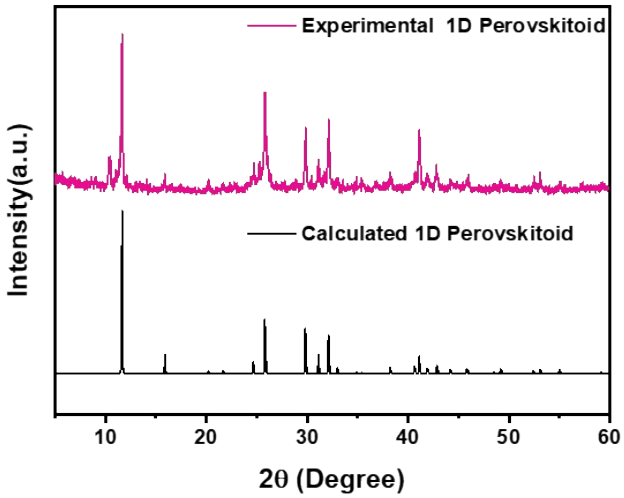

Fig. S2. PXRD patterns of the calculated and the experimental the PA^{+}-based 1D perovskitoid crystals.

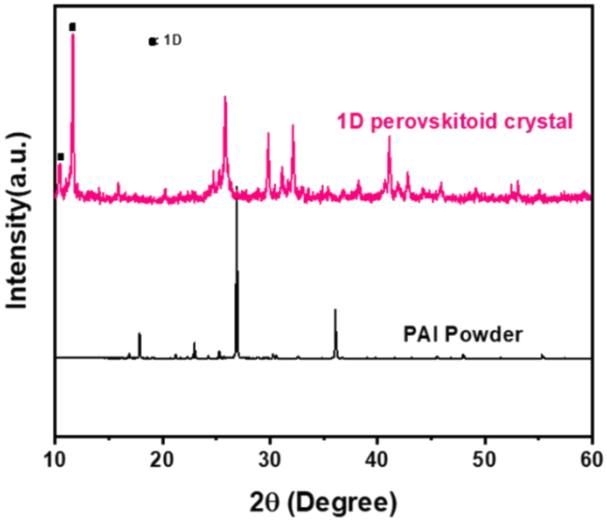

Fig. S3. PXRD patterns of the PA^{+}-based 1D perovskitoid crystals and PAI powder.

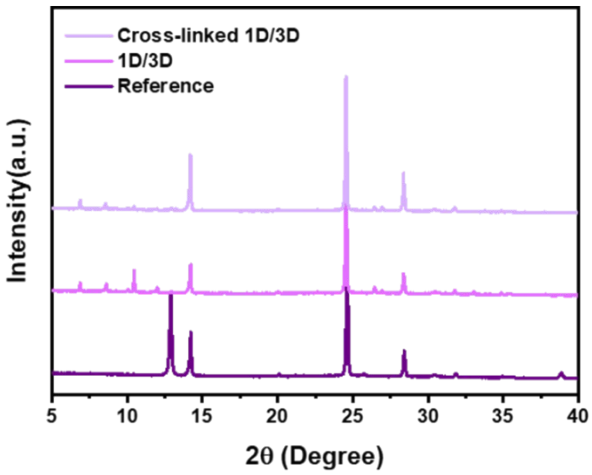

Fig. S4. XRD spectras for 1D/3D stacking and crosslink-1D/3D stacking films.

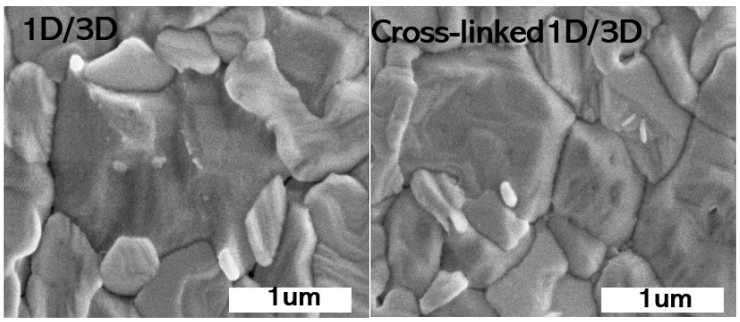

Fig. S5. The top-view SEM images of 1D/3D films before and after cross-linking.

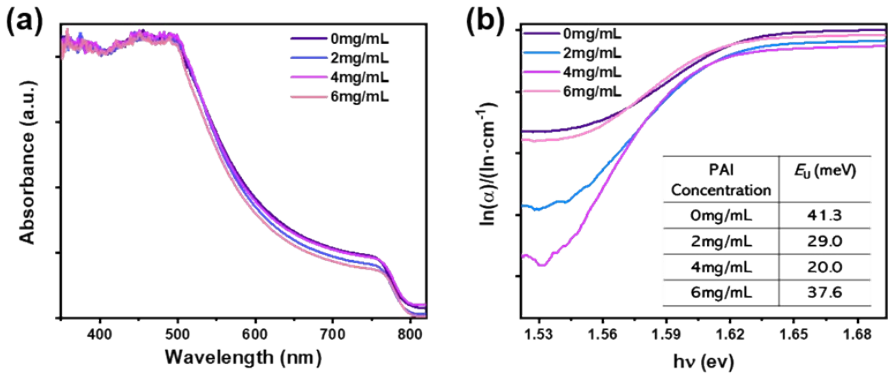

Fig. S6. The UV-vis absorption spectra and absorption coefficient derived from the UV-vis absorption spectra versus energy for PVSK films with deferent PAI concentrations, (concentration of 0, 2, 4 and 6 mg/mL) to calculate Urbach energies.

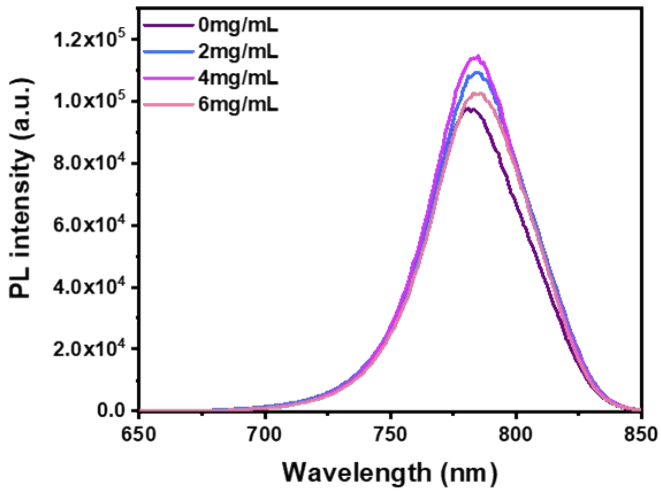

Fig. S7. The PL spectra for PVSK films with deferent PAI concentrations, (concentration of 0, 2, 4 and 6 mg/mL).

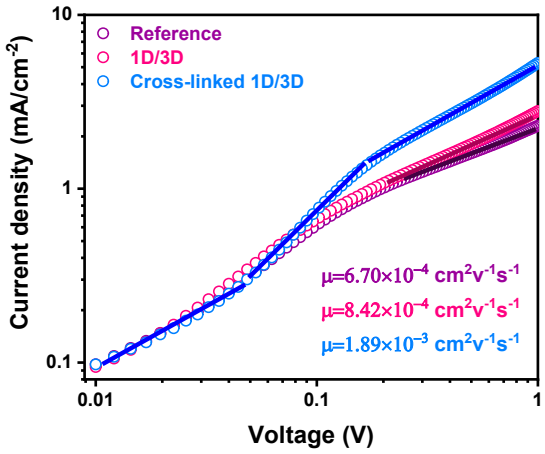

Fig. S8. The J-V characteristics of the hole-only space-charge-limited current (SCLC) devices.

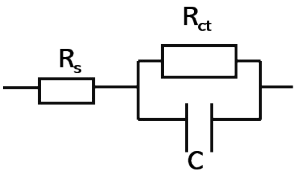

Fig. S9. The simplified equivalent circuit diagram of perovskite solar cells.

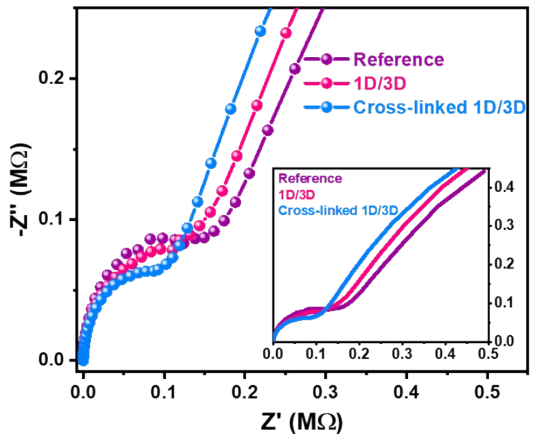

Fig. S10. EIS curves for PSCs and the inset is frequency response signal according to frequency parameter from 1MHz to 100 Hz.

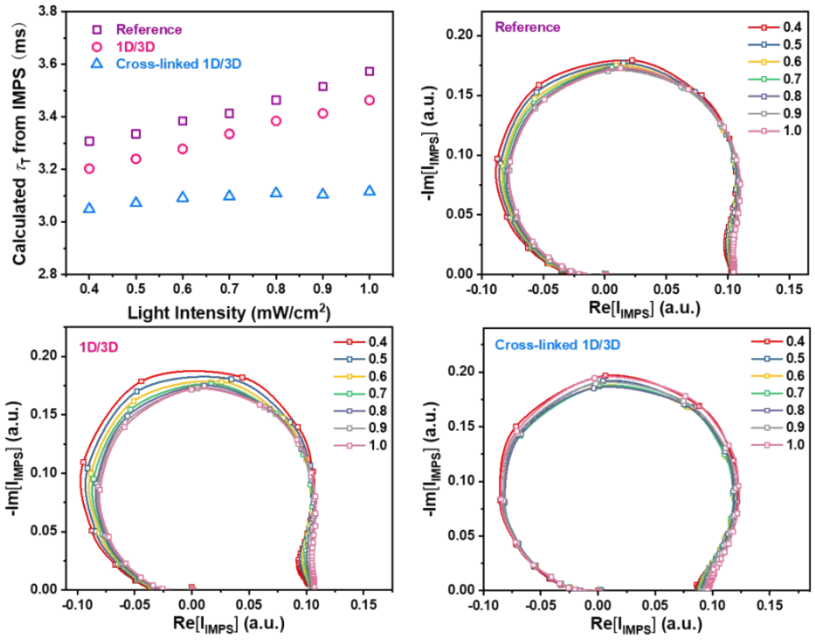

Fig. S11. The potential-modulating light intensity dependence of τ_T and Nyquist plot of the PSCs based on reference, 1D/3D and cross-linked 1D/3D.

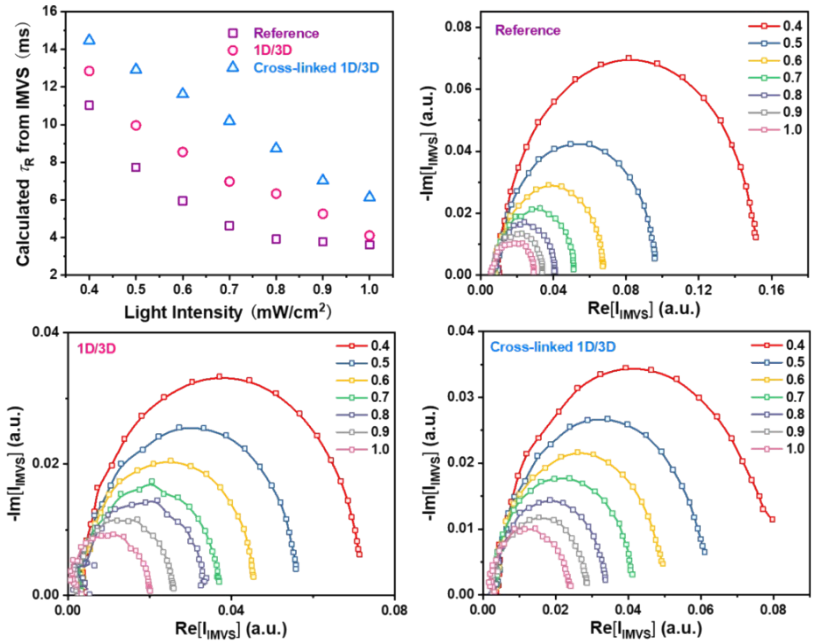

Fig. S12. The potential-modulating light intensity dependence of τ_R and Nyquist plot of the PSCs based on reference, 1D/3D and cross-linked 1D/3D.

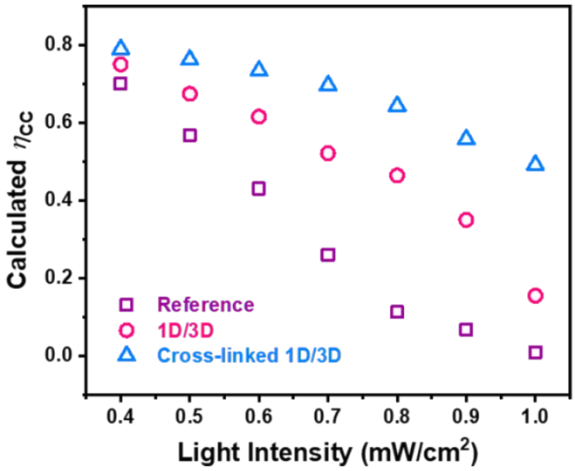

Fig. S13. The potential-modulating light intensity dependence of ηcc of the PSCs based on reference, 1D/3D and cross-linked 1D/3D.

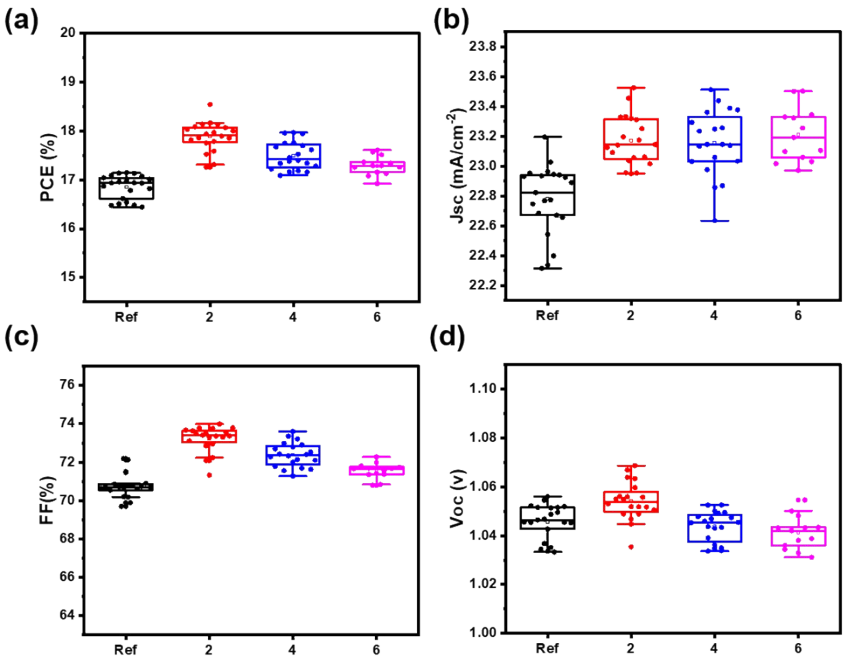

Fig. S14. Box plots of the photovoltaic parameters (V_{OC}, J_{SC}, FF, and PCE, respectively) of PSCs with different PAI concentrations (concentration of 0, 2, 4 and 6 mg/mL).

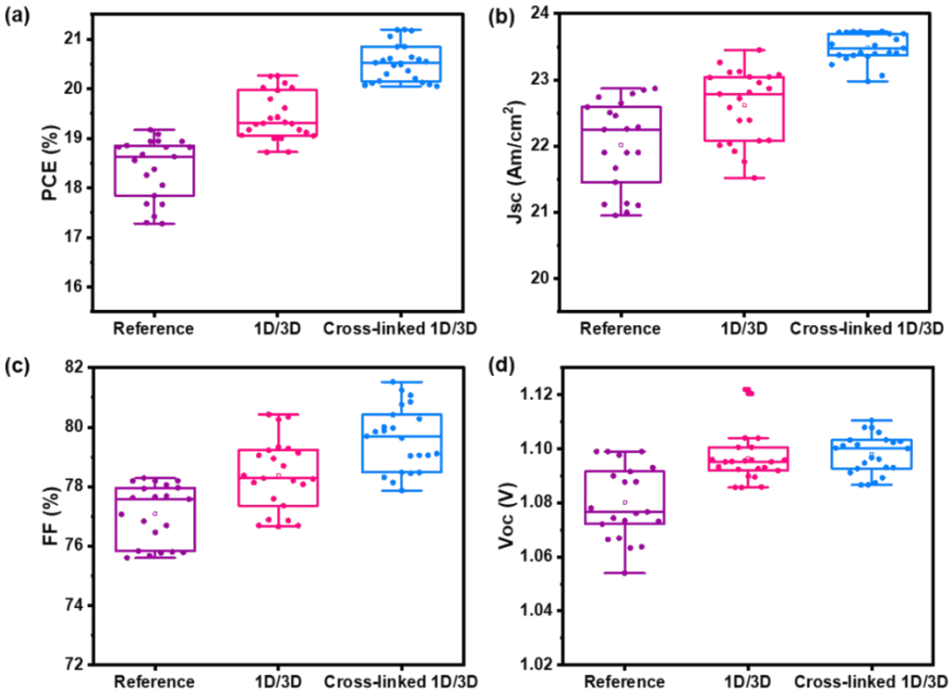

Fig. S15. Box plots of the photovoltaic parameters (V_{OC}, J_{SC}, FF, and PCE) of PSCs with different perovskite conditions.

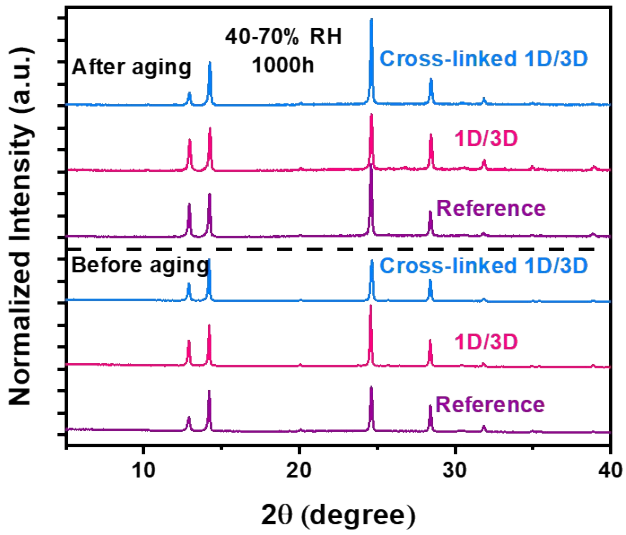

Fig. S16. XRD patterns of reference, 1D/3D and cross-linked 1D/3D perovskite films in ambient air with a relative humidity of about 40-70%, and a temperature of about 25-40 °C.

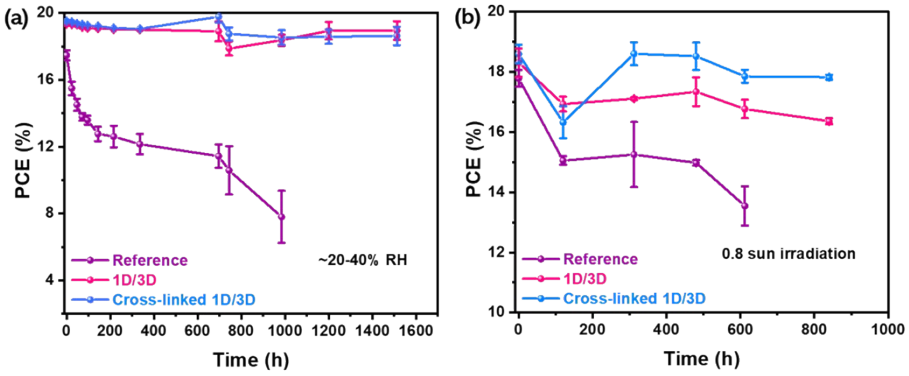

Fig. S17. (a) ISOS-D-1 stability test of the reference, 1D/3D and cross-linked 1D/3D devices before normalization stored in ambient air with a relative humidity of about 20-40%. The error bars represent the standard deviation for six separate devices (not 6 channels of the same device). (b) ISOS-L-1 stability (evolution of non-normalized PCEs of devices on continuous 0.8 sun illumination in a nitrogen atmosphere.) The error bars represent the standard deviation for six separate devices (not 6 channels of the same device)

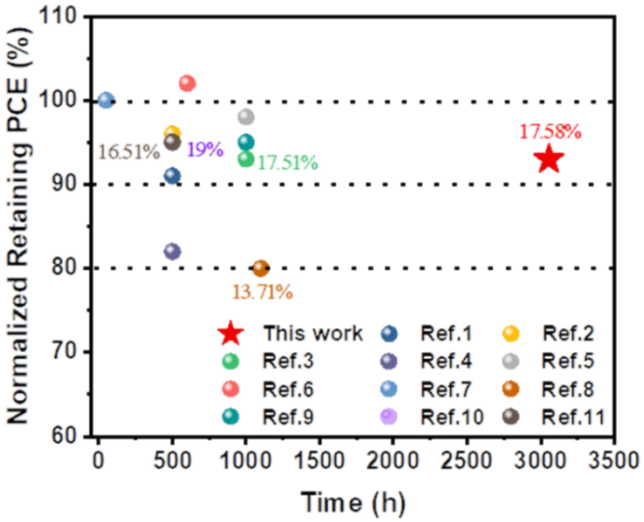

Fig. S18. MPP tracking lifetime and final PCE values from previous literatures and this work.

Table S1. Single crystal X-ray diffraction data of PA^+ based 1D perovskitoid

Identification code	1D
Empirical formula	$PAPbI_3$
Formula weight	628.70
Temperature/k	153.15
Space group	P-3
a/Å	8.77950
b/Å	8.77950
c/Å	8.19640
α/°	90.0000
β/°	90.0000
γ/°	120.0000
Volume/Å3	547.1335
Radiation	MoKα (λ = 0.71073)
2 θ range for data collection/°	5 to 80

Table S2. TRPL decay time fitted by using a bi-exponential equation.

Sample	A_1	τ_1 (ns)	A_2	τ_2(ns)	τ_{avg}(ns)	$\chi 2$
Reference/HTM	0.29	18.64	0.43	152.84	142.64	0.987
1D/3D/HTM	0.35	5.81	0.52	88.21	84.71	0.990
Cross-linked 1D/3D/HTM	0.36	2.57	0.57	49.84	48.34	0.993

The TRPL decay curves were fitted by using a bi-exponential equation

$$f(t) = A_1 \times e^{\frac{-t}{\tau_1}} + A_2 \times e^{\frac{-t}{\tau_2}}$$

where A_1 and A_2 are the relative amplitude fraction for each decay component and τ_1 and τ_2 are the fast and slow decay PL species and B is a constant. The average PL lifetime is determined by the equation

$$\tau_{avg} = \frac{A_1\tau_1^2 + A_2\tau_2^2}{A_1\tau_1 + A_2\tau_2}$$

Table S3. Average device performance of perovskite solar cells with deferent PAI concentrations, concentration of 0, 2, 4 and 6 mg/mL.

Device	V_{OC} (V)	J_{SC} (mA/cm^2)	FF (%)	PCE (%)
Reference	1.05 ± 0.01	22.78 ± 0.23	70.75 ± 0.63	16.85 ± 0.24
2 mg/ml	1.05 ± 0.01	23.17 ± 0.16	73.22 ± 0.64	17.50 ± 0.28
4 mg/ml	1.04 ± 0.01	23.16 ± 0.21	72.38 ± 0.62	17.29 ± 0.19
6 mg/ml	1.04 ± 0.01	23.21 ± 0.17	71.55 ± 0.40	17.09 ± 0.29

Table S4. Average device performance of perovskite solar cells with different conditions.

Device	Voc (V)	Jsc (mA/cm^2)	FF (%)	PCE (%)
Reference	1.08 ± 0.01	22.02 ± 0.63	77.09 ± 0.96	18.39 ± 0.59
1D/3D	1.09 ± 0.01	22.61 ± 0.51	78.38 ± 1.13	19.43 ± 0.45
Cross-linked 1D/3D	1.10 ± 0.01	23.49 ± 0.20	79.61 ± 1.02	20.53 ± 0.36

Table S5. The lifetime chart of MPP tracking for n-i-p PSCs device without encapsulation.

Test ID	Test Condition (MPP tracking)	Time	Retention PCE	Final PCE	Ref.
ISOS-L-1	N_2 filled glove-box	3055 h	93%	17.58%	This work
ISOS-L-1	N_2 filled glove-box	500 h	91%	N/A	Ref.1
ISOS-L-1	N_2 filled glove-box	500 h	96%	N/A	Ref.2
ISOS-L-1	N_2 filled glove-box	1000 h	93%	17.51%	Ref.3
ISOS-L-1	N_2 filled glove-box	500 h	82%	N/A	Ref.4
ISOS-L-2	Ar filled glove-box, 55-60 °C	1000 h	98%	N/A	Ref.5
ISOS-L-1	N_2 filled glove-box, 25 °C	600 h	102%	N/A	Ref.6
ISOS-L-1	N_2 filled glove-box	50 h	100%	N/A	Ref.7
ISOS-L-2	Ar filled glove-box, 60 °C	1100 h	80%	13.71%	Ref.8
ISOS-L-2	N_2 filled glove-box, 60 °C	1000 h	95%	N/A	Ref.9
ISOS-L-1	N_2 filled glove-box	500 h	95%	19%	Ref.10
ISOS-L-2	N_2 filled glove-box, 85 °C	500h	95%	16.51%	Ref.11
ISOS-L: Light soaking tests, 'Laboratory weathering' in the original ISOS protocols.[14,15]					

References

1. L. Wang, H. Zhou, J. Hu, B. Huang, M. Sun, B. Dong, G. Zheng, Y. Huang, Y. Chen, L. Li, Z. Xu, N. Li, Z. Liu, Q. Chen, L.-D. Sun and C.-H. Yan, *Science*, 2019, **363**, 265.
2. M. M. Tavakoli, M. Saliba, P. Yadav, P. Holzhey, A. Hagfeldt, S. M. Zakeeruddin and M. Grätzel, *Adv. Energy Mater.*, 2019, **9**, 1802646.
3. S.-H. Turren-Cruz, A. Hagfeldt and M. Saliba, *Science*, 2018, **362**, 449.
4. M. M. Tavakoli, W. Tress, J. V. Milić, D. Kubicki, L. Emsley and M. Grätzel, *Energy Environ. Sci.*, 2018, **11**, 3310.
5. D. Bi, X. Li, J. V. Milić, D. J. Kubicki, N. Pellet, J. Luo, T. LaGrange, P. Mettraux, L. Emsley, S. M. Zakeeruddin and M. Grätzel, *Nat. Commun.*, 2018, **9**, 4482.
6. J.-Y. Seo, H.-S. Kim, S. Akin, M. Stojanovic, E. Simon, M. Fleischer, A. Hagfeldt, S. M. Zakeeruddin and M. Grätzel, *Energy Environ. Sci.*, 2018, **11**, 2985.
7. M. I. Saidaminov, J. Kim, A. Jain, R. Quintero-Bermudez, H. Tan, G. Long, F. Tan, A. Johnston, Y. Zhao, O. Voznyy and E. H. Sargent, *Nat. Energy*, 2018, **3**, 648.
8. A. D. Jodlowski, C. Roldán-Carmona, G. Grancini, M. Salado, M. Ralaiarisoa, S. Ahmad, N. Koch, L. Camacho, G. de Miguel and M. K. Nazeeruddin, *Nat. Energy*, 2017, **2**, 972.
9. N. Arora, M. I. Dar, A. Hinderhofer, N. Pellet, F. Schreiber, S. M. Zakeeruddin and M. Grätzel, *Science*, 2017, **358**, 768.
10. H. Tan, A. Jain, O. Voznyy, X. Lan, F. P. García de Arquer, J. Z. Fan, R. Quintero-Bermudez, M. Yuan, B. Zhang, Y. Zhao, F. Fan, P. Li, L. N. Quan, Y. Zhao, Z.-H. Lu, Z. Yang, S. Hoogland and E. H. Sargent, *Science*, 2017, **355**, 722.
11. M. Saliba, T. Matsui, K. Domanski, J.-Y. Seo, A. Ummadisingu, S. M. Zakeeruddin, J.-P. Correa-Baena, W. R. Tress, A. Abate, A. Hagfeldt and M. Grätzel, *Science*, 2016, **354**, 206.
12. Q. Jiang, Y. Zhao, X. Zhang, X. Yang, Y. Chen, Z. Chu, Q. Ye, X. Li, Z. Yin and J. You, *Nat. Photonics*, 2019, **13**, 460.
13. Q. Dong, Y. Fang, Y. Shao, P. Mulligan, J. Qiu, L. Cao and J. Huang, *Science*, 2015, **347**, 967.
14. M. O. Reese, S. A. Gevorgyan, M. Jørgensen, E. Bundgaard, S. R. Kurtz, D. S. Ginley, C. Dana, T. L. Matthew, M. Pasquale, A. K. Eugene, E. Andreas, H. Olivier, R.C. Travis, S. Vishal, H. Martin, R. Moritz, K. KirilR., Tr. Gregor, C.K. Frederik and A. Elschner, *Sol. Energy Mater. Sol. Cells,* 2011, **95**, 1253-1267.
15. M. V. Khenkin, E. A. Katz, A. Abate, G. Bardizza, J. J. Berry, C. Brabec, F. Brunetti, V. Bulović, Q. Burlingame, A. Di Carlo, R. Cheacharoen, Y.-B. Cheng, A. Colsmann, S. Cros, K. Domanski, M. Dusza, C. J. Fell, S. R. Forrest, Y. Galagan, D. Di Girolamo, M. Grätzel, A. Hagfeldt, E. von Hauff, H. Hoppe, J. Kettle, H. Köbler, M. S. Leite, S. Liu, Y.-L. Loo, J. M. Luther, C.-Q. Ma, M. Madsen, M. Manceau, M. Matheron, M. McGehee, R. Meitzner, M. K. Nazeeruddin, A. F. Nogueira, Ç. Odabaşı, A. Osherov, N.-G. Park, M. O. Reese, F. De Rossi, M. Saliba, U. S. Schubert, H. J. Snaith, S. D. Stranks, W. Tress, P. A. Troshin, V. Turkovic, S. Veenstra, I. Visoly-Fisher, A. Walsh, T. Watson, H. Xie, R. Yıldırım, S. M. Zakeeruddin, K. Zhu and M. Lira-Cantu, *Nat. Energy,* 2020, **5**, 35-49.